UC Riverside
UC Riverside Previously Published Works

Title

Velocity-selective arterial spin labeling perfusion MRI: A review of the state of the art and recommendations for clinical implementation

Permalink

https://escholarship.org/uc/item/00v0358t

Journal

Magnetic Resonance in Medicine, 88(4)

ISSN

0740-3194

Authors

Qin, Qin
Alsop, David C
Bolar, Divya S
et al.

Publication Date

2022-10-01

DOI

10.1002/mrm.29371

Copyright Information

This work is made available under the terms of a Creative Commons Attribution-NonCommercial-NoDerivatives License, available at https://creativecommons.org/licenses/by-nc-nd/4.0/

Peer reviewed

eScholarship.org Powered by the California Digital Library
University of California

Received: 12 March 2022 | Revised: 16 May 2022 | Accepted: 8 June 2022 | Published on: 12 July 2022

DOI: 10.1002/mrm.29371

GUIDELINES

Magnetic Resonance in Medicine

Velocity-selective arterial spin labeling perfusion MRI: A review of the state of the art and recommendations for clinical implementation

Qin Qin[1] | David C. Alsop[2] | Divya S. Bolar[3] | Luis Hernandez-Garcia[4] | James Meakin[5] | Dapeng Liu[1] | Krishna S. Nayak[6] | Sophie Schmid[7] | Matthias J. P. van Osch[7] | Eric C. Wong[3] | Joseph G. Woods[3] | Greg Zaharchuk[8] | Moss Y. Zhao[8] | Zungho Zun[9] | Jia Guo[10] | on Behalf of the ISMRMPerfusion Study Group

[1]The Russell H. Morgan Department of Radiology and Radiological Science, Johns Hopkins University School of Medicine, Baltimore, Maryland, USA

[2]Department of Radiology, Beth Israel Deaconess Medical Center and Harvard Medical School, Boston, Massachusetts, USA

[3]Center for Functional Magnetic Resonance Imaging, Department of Radiology, University of California, San Diego La Jolla, California, USA

[4]FMRI Laboratory, University of Michigan, Ann Arbor, Michigan, USA

[5]Department of Radiology, Nuclear Medicine and Anatomy, Radboud University Medical Center, Nijmegen, The Netherlands

[6]Magnetic Resonance Engineering Laboratory, Ming Hsieh Department of Electrical Engineering, University of Southern California, Los Angeles California, USA

[7]C.J. Gorter Center for high field MRI, Department of Radiology, Leiden University Medical Center, Leiden, The Netherlands

[8]Department of Radiology, Stanford University, Stanford, California, USA

[9]Department of Radiology, Weill Cornell Medicine, New York, New York, USA

[10]Department of Bioengineering, University of California Riverside, Riverside, California, USA

Correspondence
Qin Qin, The Russell H. Morgan Department of Radiology and Radiological Science, Johns Hopkins University School of Medicine, Baltimore, Maryland, USA.
Email: qqin1@jhu.edu

Funding information
National Heart, Lung, and Blood Institute, Grant/Award Numbers: R01 HL138182, R01 HL144751, R01HL130494; National Institute of Biomedical Imaging and Bioengineering, Grant/Award Numbers: R01-EB025220, P41EB031771; National Institute of Child Health and Human Development, Grant/Award Number: R01HD100012; Netherlands Organization for Scientific Research, Grant/Award Numbers: VENI-project17319, Vici-projectnumber016.160.351; National Institute of Neurological Disorders and Stroke, Grant/Award Number: R01NS112233; American Heart Association, Grant/Award Number: 826254; Greg Zaharchuk, Grant/Award Number: NIH R01-EB025220

Abstract

This review article provides an overview of the current status of velocity-selective arterial spin labeling (VSASL) perfusion MRI and is part of a wider effort arising from the International Society for Magnetic Resonance in Medicine (ISMRM) Perfusion Study Group. Since publication of the 2015 consensus paper on arterial spin labeling (ASL) for cerebral perfusion imaging, important advancements have been made in the field. The ASL community has, therefore, decided to provide an extended perspective on various aspects of technical development and application. Because VSASL has the potential to become a principal ASL method because of its unique advantages over traditional approaches, an in-depth discussion was warranted. VSASL labels blood based on its velocity and creates a magnetic bolus immediately proximal to the microvasculature within the imaging volume. VSASL is, therefore, insensitive to transit delay effects, in contrast to spatially selective pulsed and (pseudo-) continuous ASL approaches. Recent technical developments have improved the robustness and the labeling efficiency of VSASL, making it a potentially more

This is an open access article under the terms of the Creative Commons Attribution-NonCommercial-NoDerivs License, which permits use and distribution in any medium, provided the original work is properly cited, the use is non-commercial and no modifications or adaptations are made.
© 2022 The Authors. *Magnetic Resonance in Medicine* published by Wiley Periodicals LLC on behalf of International Society for Magnetic Resonance in Medicine.

favorable ASL approach in a wide range of applications where transit delay effects are of concern. In this review article, we (1) describe the concepts and theoretical basis of VSASL; (2) describe different variants of VSASL and their implementation; (3) provide recommended parameters and practices for clinical adoption; (4) describe challenges in developing and implementing VSASL; and (5) describe its current applications. As VSASL continues to undergo rapid development, the focus of this review is to summarize the fundamental concepts of VSASL, describe existing VSASL techniques and applications, and provide recommendations to help the clinical community adopt VSASL.

KEYWORDS

arterial spin labeling, arterial transit delay, cerebral blood flow, perfusion, velocity selective arterial spin labeling, velocity selectivity

1 | INTRODUCTION

Arterial spin labeling (ASL) MRI is a unique imaging method that creates sensitivity to tissue perfusion without contrast injection or ionizing radiation. Quantitative perfusion imaging using ASL has proven to be useful for both research and clinical applications in the brain and beyond,[1,2] because it provides access to a physiological quantity that is critical to the nutritive supply to tissues. The key distinguishing feature of ASL is the labeling: magnetic field gradients and radiofrequency pulses are used to differentially affect the magnetization of tissue and arterial blood. As the altered blood magnetization enters the microvasculature and tissue, it causes a measurable change in tissue magnetization. The difference between such a labeled image and a second image with different labeling, often called the control image, yields a perfusion-sensitive image.

Labeling of arterial blood in ASL is achieved by exploiting the fact that blood is moving. Spatially selective ASL aims to generate a difference in magnetization between spins outside the image volume (Figure 1), where the feeding arteries are located, and those in the tissue within the imaged volume. Subsequently, inflow of the labeled spins into the imaging volume provides the perfusion-weighted signal. Spatial selective labeling can be achieved by continuous labeling of arterial blood as it flows through a plane close to the imaging volume or by a short sequence of pulses that labels spins over a wide region below or surrounding the imaging plane. Pseudo-continuous labeling (PCASL)[3] has proven a robust approach to labeling and has been recommended for most ASL applications.[1]

However, the primary weakness of spatially selective ASL is the decay of the label as it flows from the larger arteries where blood is labeled, into the microvasculature and tissue. Because the duration of this arterial transit time (ATT) can be comparable to or longer than the T_1 of blood, significant signal can be lost because of this decay. Moreover, uncertainty in the ATT complicates quantification and sequence optimization. A post-labeling delay (PLD) longer than any expected ATT can be used with PCASL to reduce the impact of this uncertainty.[4] However, because signal loss increases as PLD increases, PLDs recommended for clinical application are short enough to maintain adequate signal, but often too short for accurate quantitation in diseases commonly seen clinically, such as acute ischemic stroke and carotid stenosis. More complex approaches involving multiple delays can be used to optimize results for each subject and can also be used to provide potentially useful maps of ATT and arterial blood volume, but they cannot address the fundamental loss of signal because of ATT. In steno-occlusive pathologies, such as acute ischemic stroke, moyamoya, and carotid stenosis, even multiple or long delay approaches cannot be used to accurately image cerebral blood flow (CBF) when transit delays are severe.[5]

Alternative labeling approaches that are based on arterial blood velocity and not spatial location provide an opportunity to reduce or eliminate ATT related signal loss and uncertainties. Because the labeling is not limited by spatial location, velocity selective (VS) labeling can be applied to the imaged volume itself (Figure 1). If the velocity encoding reaches low enough velocities, it can label within or close to the slowly moving blood of the microvasculature, essentially eliminating any ATT. The signal change from pulsed VS labeling is competitive with PCASL in volumetric imaging of normal subject brains and may perform even better in patients with long delays because of proximal stenosis and/or circuitous collateral flow. The potential benefit may be even greater in organs outside the brain where the transit time from a major arterial vessel is longer, or the arterial supply is complex.

In this review, we describe the theoretical basis for VSASL and the dominant VS labeling strategies, including

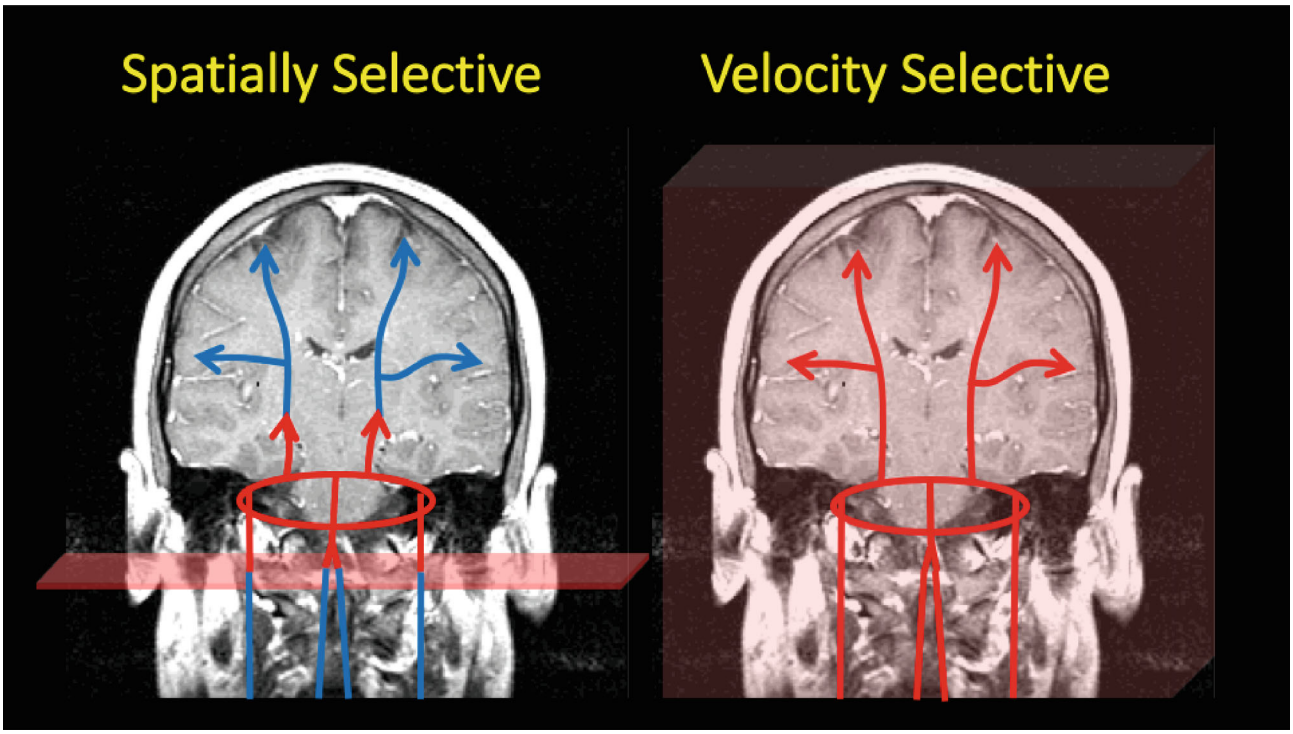

FIGURE 1 A simple cartoon depicting the differences between spatially selective and velocity selective labeling. The cartoon represents blood in the carotid and vertebral arteries flowing into the circle of Willis, which in turn distributes blood to the rest of the brain. In the left panel, inflowing spins are labeled as they flow through a labeling plane (such as in pseudo-continuous arterial spin labeling [PCASL]), defined by the pulse. The labeling process is depicted by a color change from blue to red. The cartoon depicts the label at the beginning of the labeling pulse. However, the pulse is applied for an extended period such that the labeled spins fill the vascular space. The time between the spins being labeled at the neck and their arrival to the tissue is referred to as the arterial transit time and a significant amount of the label is lost because of T_1 relaxation. In contrast, velocity selective pulses label spins depending on their velocity, and not their location, as depicted in the right panel. As a result, the vascular space is immediately filled with labeled spins and the arrival time of the leading edge of the label to the tissue is dramatically reduced

model validation and methods for quantification. We, then, explore practical issues of implementation and application, including ways to optimize labeling efficiency and reliability, while controlling vulnerability to tissue motion and RF/gradient imperfections. Incorporating background suppression (BS) to increase robustness and achieving high quality large spatial coverage is also discussed. Finally, we survey recent applications of VSASL.

2 | KINETIC MODELS

VSASL labels arterial blood moving above a chosen velocity, referred to as the cutoff velocity (V_{cut}, defined below), by a short (on the order of tens of milliseconds) train of RF and flow-sensitive gradient pulses. During imaging, spins flowing above the same V_{cut} are saturated so that only the labeled arterial blood that decelerates below the V_{cut} is measured. The cutoff velocity, V_{cut}, determines how deep into the arterial tree the blood is labeled and a sufficiently low value will ensure that this boundary occurs close to the microvasculature/tissue within the imaging volume. Therefore, ATT = 0 s can in principle be achieved across the entire imaging volume, and a 0 PLD can be implemented to minimize ASL signal decay because of T_1 relaxation, providing an signal-to-noise ratio (SNR) advantage and potentially higher quantification accuracy, especially when long transit delays are expected. A comparison between the arterial input functions and the time courses of the ASL signals using pulsed ASL (PASL), PCASL and VSASL is demonstrated in Figure 2. Two main approaches for VSASL, VS saturation (VSS) and VS inversion (VSI), are displayed.

3 | PULSE SEQUENCE DESIGN OF VSASL

A typical VSASL pulse sequence diagram is shown in Figure 3. A global saturation module at the beginning of the TR (or right after the image acquisition) resets the arterial magnetization to a known state to avoid spin

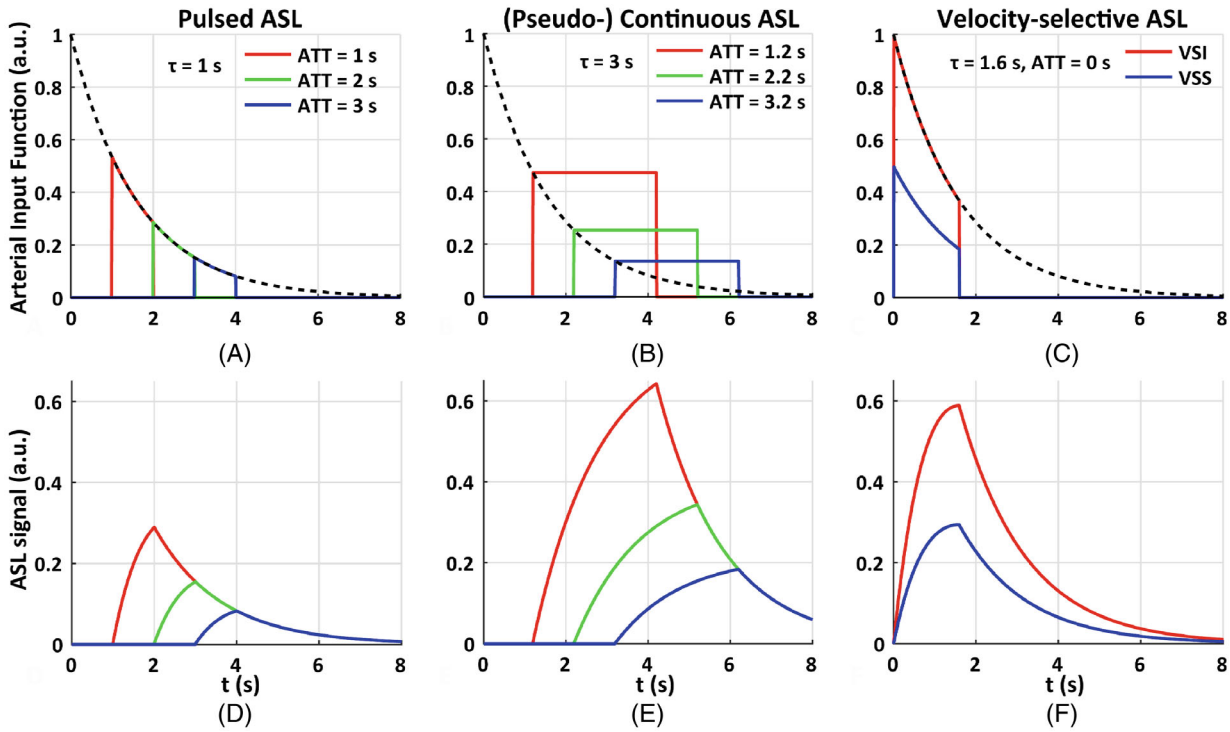

FIGURE 2 The arterial input function of (A) pulsed arterial spin labeling (PASL) with the temporal width of the labeling bolus τ of 1.0 s, arterial transit time (ATT) of 1.0, 2.0, 3.0 s; (B) pseudo-continuous ASL (PCASL) with the labeling duration τ of 3.0 s, ATT of 1.2, 2.2, and 3.2 s; and (C) velocity-selective ASL (VSASL) with VS saturation (VSS) and VS inversion (VSI) pulses, and ATT of 0 s, the temporal width of the labeling bolus τ of 1.6 s. In this illustration of ideal conditions, t is the time from the start of the labeling pulse, the labeling efficiency $\alpha = 1.0$ (for VSS, $\alpha = 0.5$), $M_0 = 1$, $T_1 = 1.6$ s. Their corresponding kinetic curves indicate that the maximal perfusion-weighted signal of pulsed ASL (D) is only half of that of PCASL (E), and both are sensitive to ATT. In contrast, the ATT for VSASL (F) is essentially 0 and the maximal signal of VSI is about (or more than) twice that of PCASL when the ATT of PCASL is longer than 2.2 s. This figure demonstrates that, with its full potential reached, VSASL has minimal susceptibility to ATT effects among existing methods and has a significant signal advantage especially when long ATTs with PASL or PCASL are expected

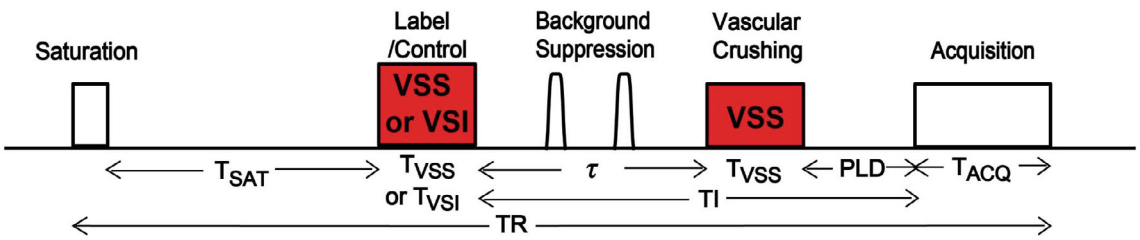

FIGURE 3 Typical pulse sequence diagram of velocity-selective arterial spin labeling (VSASL). The labeling and vascular crushing modules (VCM) with a matched V_{cut} are shown in red

history effects.[6] After a saturation time (T_{sat}), the VS labeling (label/control) module (VSS or VSI) labels the arterial spins. A delay (τ) then follows, which allows labeled spins to flow into and accumulate in the tissue of interest. A vascular crushing module (VCM) with the same V_{cut} for imaging as for labeling is then applied and defines the temporal width of the VSASL bolus (with τ reflecting the bolus duration), similar to how QUIPSS II determines the temporal width in PASL.[7] The VCM saturates the spins moving above V_{cut}, therefore, only the arterial blood decelerated below V_{cut} after the labeling will generate measurable ASL signal. It can be implemented either as a VSS label module before the image acquisition or flow-crushing gradients in the acquisition. The PLD is defined as the delay between the VCM and the image acquisition thereby consistent across all ASL methods. When the VCM is applied right before acquisition or implemented in the form of flow-crushing gradients between the excitation and acquisition, the PLD is effectively 0. The inflow time (TI) is the time from the application of the labeling module to

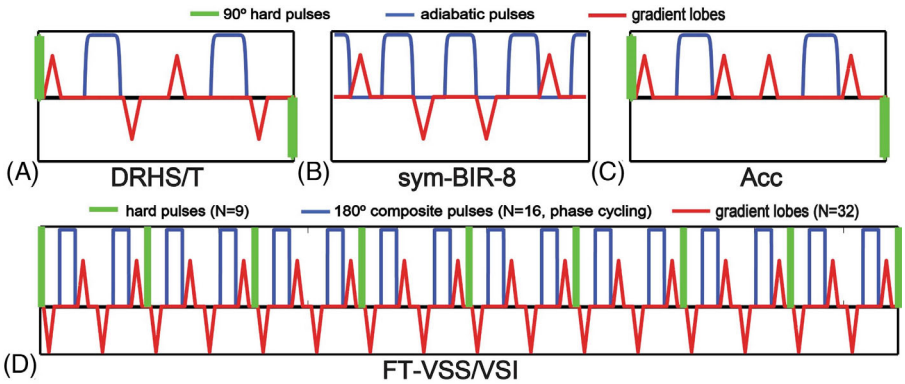

FIGURE 4 Diagrams of (A) double-refocused hyperbolic-secant (DRHS) or double-refocused hyperbolic-tangent (DRHT); (B) symmetric (sym-) BIR-8; (C) Acceleration (Acc)-based; (D) Fourier-transform velocity selective saturation (FT-VSS) or Fourier-transform velocity selective inversion (FT-VSI)

the image acquisition, and equals τ when the PLD is 0. To improve the SNR, background suppression pulses are usually inserted during TI.

4 | VELOCITY SELECTIVE MODULES

In general, VS modules consist of RF and flow-sensitive gradient pulses. Bipolar gradient lobes, or paired monopolar lobes surrounding a refocusing pulse, can generate a velocity-dependent phase for flowing spins. This approach was first used between excitation and acquisition as a "crusher" to attenuate large-vessel signals for perfusion estimation.[8–10] Incorporation of motion-sensitized gradients in excitation, saturation, or inversion RF composite pulses was then proposed as VS pulse trains,[11] and VSASL perfusion imaging was first suggested by the authors as an application.

In VSASL, the RF pulses remain the same under both the label and the control conditions. For the flow-sensitive gradient pulses, a non-0 first moment and a 0 first moment is required for the label and the control conditions, respectively. For the control condition, the flow-sensitive gradient pulses can either be all turned off or flow-compensated. Controls with gradients turned off (velocity-insensitive) are typically applied in VSS implementation for its simplicity. Controls with velocity-compensated gradient configurations are often used in VSI-based labeling. The benefits and drawbacks of the 2 control designs are discussed in the VSI section below.

5 | VELOCITY SELECTIVE SATURATION PULSE TRAINS

The first in vivo implementation of VSASL, proposed by Wong et al,[12] used a single segment ($90°_x$, G_+, $180°_y$, G_+, $90°_{-x}$) spin-echo pulse train with hard RF pulses. A single segment module, such as this, results in a cosine modulation in Mz across velocities. Under the assumption of laminar flow, this modulation becomes a sinc function, with its first 0 crossing at V_{cut}. To a first order approximation, this modulation can be considered to saturate spins moving above V_{cut}, while leaving static spins unperturbed.

The use of a single 180° B_1-sensitive refocusing pulse (e.g., hard pulse) in this VS module made the spin-echo sensitive to B_1^+ variation,[13] so later implementations used adiabatic pulses for refocusing,[6] which can be designed to be extremely robust to B_1^+ variation. Adiabatic pulses impart a nonlinear phase across resonance frequencies, so such pulses must be used in pairs to reverse this phase accrual, resulting in a ($90°_x$, G_+, $180°_a$, $180°_a$, G_-, $90°_{-x}$) sequence. Wong et al[6] noted that a quadrapolar gradient scheme could be used to reduce eddy current errors in a similar way to Reese et al,[14] resulting in a ($90°_x$, G_+, $180°_a$, G_-, G_+, $180°_a$, G_-, $90°_{-x}$) module. This module is commonly referred to as a double-refocused hyperbolic-secant (DRHS) module or double-refocused hyperbolic-tangent (DRHT) if hyperbolic-tangent refocusing pulses are used[15] (Figure 4A).

The DRHS/T module robustly minimizes sensitivity to off-resonance and ECs. However, the use of B_1^+-sensitive pulses for the excitations results in labeling efficiency that depends on the spatially non-uniform B_1^+, leading to a systematic underestimation of perfusion.

To overcome this limitation, Wong and Guo[16] proposed the use of adiabatic pulses, such as BIR-4 pulses,[17] with velocity sensitizing gradients between RF pulses: ($90°_a$, G_+, $180°_a$, G_+, $90°_a$). Note that the nonlinear phase imparted by the single refocusing pulse is now reversed by the 2 adiabatic half-passage pulses. Despite the BIR-4 VS module being very robust to B_0 and B_1^+ variation, the use of monopolar gradients can result in very large EC effects leading to subtraction artifacts in the perfusion images.[18]

To alleviate this problem, while retaining most of the B_0 and B_1^+ robustness of the BIR-4 module, Meakin and Jezzard[18] proposed an asymmetric BIR-8 (asym-BIR-8) VS module with gradients at 3 of the 4 0-RF intervals, in a similar pattern to[6] for reducing EC errors: ($90°_a$, $180°_a$, G_+, $180°_a$, G_-, G_+, $180°_a$, G_-, $90°_a$).

Guo et al[19] further improved on this design with the symmetric BIR-8 (sym-BIR-8) VS module (Figure 4B), placing 1 gradient in each of the 0-RF intervals ($90°_a$, G_+, $180°_a$, G_-, $180°_a$, G_-, $180°_a$, G_+, $90°_a$), which was found to further reduce EC errors. The authors additionally showed that inserting time delays after each of the gradient pulses could further reduce EC errors, albeit at the cost of increased T_2 decay and reduced labeling efficiency.

6 | VELOCITY SELECTIVE INVERSION PULSE TRAINS

The technical advancement of the VSS pulses mentioned above has significantly improved their robustness against B_0 and B_1^+ variations and EC effects. However, because of less efficient labeling by saturation (half of the labeling efficiency as compared to labeling by inversion), VSS-based VSASL typically has a lower SNR efficiency ($\text{SNR}/\sqrt{\text{acquisition time}}$) than conventional inversion-based labeling methods (PASL and PCASL) when ATTs are in the typical physiological range (e.g., <2 s).[6,20,21] To improve the labeling efficiency, research efforts have been made to develop VSI pulses.

The first VSI implementation proposed by Wong and Guo,[22] used 2 or 3 modules of the DRHS/T pulse trains, following the modular approach of Norris et al.[11] With modified flip angles and phases in the hard RF pulses in the form of ($\alpha°_i$, G_+, $180°_a$, $180°_a$, G_-, $\beta°_i$) for the *i*th module, the VSI pulse trains were able to invert the moving spins within a wide range of velocities along 1 flow direction, and had demonstrated a significant SNR increase (20%-30%) in gray matter compared to VSS-based labeling. However, the velocity response is not ideal and the pulse train is sensitive to B_1^+ inhomogeneity because of the hard pulses involved.

A more recent Fourier-transform-based velocity selective (FT-VS) pulse implementation[15] builds on the excitation *k*-space formalism[23,24] by interleaving a series of non-selective RF pulses with velocity-encoding gradients. This approach can theoretically produce almost arbitrary VS profiles. In the small tip angle approximation,[23] this VS profile is proportional to the Fourier transform of the set of flip angles of RF pulses applied at the beginning of consecutive velocity-encoding steps.

A challenge to the FT-VS method has been its sensitivity to imperfections in B_0 and B_1^+. The original scheme[25] did not include any refocusing pulses, which effectively shifted its excitation profile along the velocity direction in proportion to B_0 off-resonance.[26] To alleviate this susceptibility to B_0 field inhomogeneity, Shin et al[27] incorporated 1 composite refocusing pulse within each velocity-encoding step and modified the RF and gradient waveforms accordingly. For improved immunity to B_0/B_1^+ field inhomogeneities, Qin et al[28] proposed paired refocusing pulses within each velocity-encoding step accompanied with phase-cycling of refocusing pulses through the FT-VS pulse trains (Figure 4D).

Fourier-transform velocity selective inversio (FT-VSI) based VSASL for CBF quantification was first demonstrated by Qin and van Zijl[15] using nine 20° excitation pulses (rectangular modulation) with block refocusing pulses. Later, FT-VSI labeling was also implemented with composite refocusing pulses for more robustness to both B_1^+ field inhomogeneity and eddy-current,[29,30] and with sinc modulation of the excitation pulses for smoother VS profiles.[30,31] In practice, current FT-VSI implementations can offer 20% to 40% increase in SNR compared to VSS labeling.[15,30,32]

Note that the design of the control module is another important consideration for the performance of VSI-ASL. With imperfect refocusing under poor B_0/B_1^+ conditions, a velocity-insensitive control produced by switching off velocity-encoding gradients is susceptible to both stripe artifacts[33,34] and non-0 DC bias[35] in the spatial response; whereas a velocity-compensated control produced by using unipolar gradients reduces the systematic subtraction errors from both DC bias and unbalanced diffusion attenuation, but with deteriorated VS profiles, higher sensitivity to ECs and reduced labeling efficiency.[15,35] A novel dynamic phase-cycling approach for the velocity-insensitive control module was recently proposed to mitigate the systematic quantification errors from DC bias for FT-VSI prepared VSASL.[35]

VSI-ASL has been demonstrated for CBF mapping with 3D gradient and spin echo[29] and 3D stack-of-spirals[36] readouts. Three dimensional VSI-ASL-based CBF maps in neonatal piglet brain revealed well-defined regional CBF patterns that match known functional domains.[37] Note that the calculation of the timing of BS pulses needs to take into account the varying degrees of inversion of static tissue magnetization by the VSI pulse train itself, which is sensitive to B_1^+ field inhomogeneity because of the use of hard pulses at the beginning of each velocity-encoding step.

7 | MULTI-MODULE VSASL

In addition to VSI labeling, the multi-module VSS labeling method[21] was also developed to improve the SNR efficiency of VSASL, showing an improvement of 20% to 30% compared to single-module VSS (sm-VSS) labeling. In this method, 2 effects contribute to the SNR efficiency increase: (1) additional VSS modules create larger magnetization difference between the label and the control

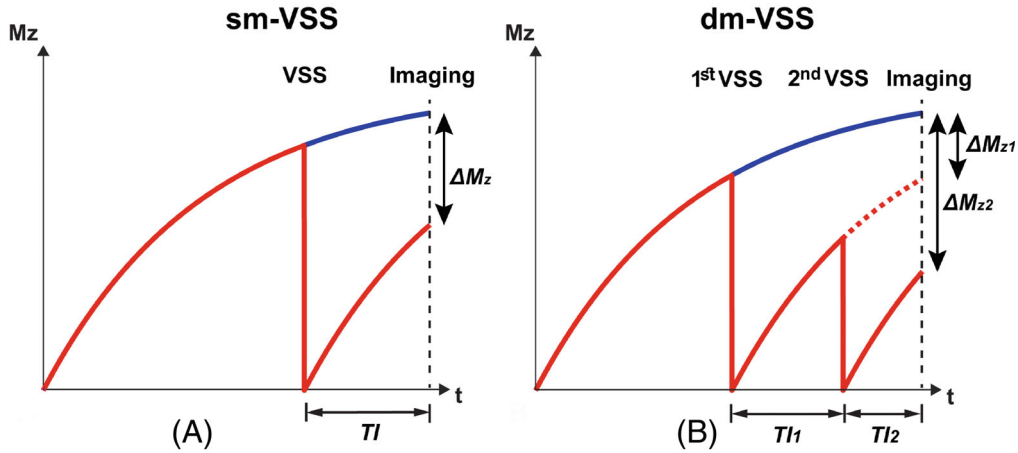

FIGURE 5 Schematics showing the arterial longitudinal magnetization (Mz) of single-module velocity selective saturation (sm-VSS) (A), and dual-module VSS (dm-VSS) labeling (B) under the label (red) and the control (blue) conditions. In dm-VSS, the dashed red curve represents the magnetization of arterial spins that are labeled by only the first VSS module (ΔM_{Z1}); the solid red curve represents those labeled by both VSS modules (ΔM_{Z2}). TI_1 and TI_2 are the inflow times between the 2 VSS modules and imaging, respectively

conditions by "re-labeling" the relaxed spins; and (2) additional VSS modules can label the arterial spins that enter the coverage of the RF transmit coil after the first VSS module, effectively increasing the temporal width of the label bolus. Generally, the first effect dominates. In practice, a dual-module VSS (dm-VSS) implementation is preferred, achieving a large SNR improvement with a limited specific absorption rate increase, whereas additional VSS modules only improve SNR efficiency marginally. A theoretical comparison of the ASL signal by sm-VSS and dm-VSS labeling is demonstrated in Figure 5. More details on modeling of the ASL signals using multi-module VSASL can be found here.[21]

At 3T, TI_1/TI_2 of 1.15/0.82 s are recommended for dm-VSS labeling, with a 23% increase of SNR efficiency measured in brain in vivo[21,30] compared to sm-VSS. In practice, it is important to use robust VSS pulses, such as the sym-BIR-8-based VSS,[19] for dm-VSS labeling; otherwise, the SNR efficiency improvement would be limited[35] because it is affected by both VSS modules. The artifactual signal from diffusion attenuation difference between the label and control conditions may be increased by dual-module labeling, especially in voxels dominated by cerebrospinal fluid (CSF), which has a much higher diffusion coefficient than gray matter and white matter. This artifact can be removed via modeling the diffusion attenuation effects[21] if partial volume fractions of tissues are known.

8 | ACCELERATION-SELECTIVE ASL

Acceleration selective ASL (Acc-ASL) is a method that effectively labels the arterial blood pool with the same advantages of VSS-ASL (i.e., creating labels closer and within the tissue under investigation). This selectivity toward arterial blood arises from a much stronger deceleration on the arterial side of the microvascular tree than acceleration on the venous side. It is important to realize that both acceleration and deceleration will lead to saturation and therefore, creation of labeled blood magnetization. As first demonstrated in ASL-based magnetic resonance angiography (MRA),[38] a flow-selective labeling module with 0 first gradient moment (m_1) (i.e., spins flowing with constant velocity will not be saturated) but a non-0 second moment (m_2), resulting in dephasing of spins based on acceleration/deceleration (Figure 4C) (i.e., Acc-ASL)[39] will mainly label the arterial side of the vascular tree. Therefore, no further suppression of venous labels is necessary, although the fact that the bolus cannot be cut off by means of a VCM complicates quantification.

The origin of the label is less clear for Acc-ASL than in VSASL, because several processes can result in effective labeling: (1) the deceleration of blood in the large arteries is probably one of the most important sources of label in Acc-ASL; (2) blood flow on the arterial side is more pulsatile than on the venous side, resulting in additional labeling; and (3) blood flow changing direction during the module duration, for example when passing through the microvasculature, will also lead to dephasing (the change in direction can be seen as deceleration in the original direction and acceleration in the new direction).

Together, these effects result in a combination of blood volume and flow dependent labeling in the arteries with almost no venous labeling, as evidenced by lack of observable Acc-ASL signal in the sagittal sinus.[39] Moreover, the amount of label created is higher than for VSS-ASL,

thereby also providing higher temporal SNR (tSNR). However, as already mentioned, quantification of perfusion is challenging. In the first paper on Acc-ASL,[39] an almost double tSNR was found compared to VSS-ASL, although a later study showed only 25% higher tSNR.[32] In the medulla of the kidney, a higher tSNR was also observed compared to VSS-ASL,[32] although tSNR was almost equal in the cortex.[32] Important to note is that Acc-ASL seems to create labels further into the vascular tree (i.e., within smaller vessels) than VSS-ASL with similar gradient amplitudes.[40] Head-to-head comparison with O^{15}-H_2O PET showed similar qualitative perfusion maps, although no attempt has yet been made to quantify Acc-ASL data.[41]

9 | RECOMMENDED PARAMETERS FOR IMAGING AND QUANTIFICATION

9.1 | Cutoff velocity (V_{cut})

As previously mentioned, a matched and sufficiently low V_{cut} for labeling and vascular crushing in imaging causes the ATT to be effectively 0 in VSASL. During labeling, the blood will accumulate a flow-dependent phase that leads to dephasing when the labeled blood mixes during the transit to the tissue/capillary bed. Therefore, a model of the velocity distribution of the arterial blood is needed to define the V_{cut} and the effective labeling bolus. Note that the velocity distribution along a given direction is also affected by the orientations of the arteries. For simplicity, a laminar flow distribution is typically assumed (e.g., for a vessel of radius R, $\mathbf{V}(r) = V_{max}[1-(r/R)^2]$ at a distance of r from the center, where V_{max} is the maximal velocity at the center and the mean velocity $V_{mean} = V_{max}/2$). Subsequently, the overall labeling effect can be approximated by an integration of the magnetization response of the laminar layers within the blood vessels.

For VSS modules that tip the magnetization into the transverse plane before any flow-sensitive gradient pulses are applied, such as DRHS/T and BIR-8, the longitudinal magnetization response is a cosine function of the velocity (V) and the first moment of the gradient pulses (m_1), $M_z = M_0\cos(\gamma m_1 V)$ (Figure 6A), where M_0 is the longitudinal magnetization at equilibrium and γ is the gyromagnetic ratio. The integration over the laminar velocity profile generates a sinc profile with respect to V_{mean}, for example, $M_z = M_0\mathrm{sinc}(2\gamma m_1 V_{mean})$ (Figure 6B).

For VS modules that gradually tip the magnetization into the transverse plane (e.g., Fourier-transform velocity selective saturation, FT-VSS) or along the Z axis (FT-VSI), their longitudinal magnetization responses are no longer a simple function of V and m_1 (Figure 6C). In addition, the inversion (or saturation) bands of FT-based VS pulses are periodic in velocity (i.e., they appear at higher velocities in addition to around 0 velocity). After integrating over a laminar flow velocity profile, the longitudinal magnetization responses with respect to V_{mean} are shown in Figure 6D.

The V_{cut} of the VCM that is played out during or just before the image acquisition, is defined as the first 0-crossing point of the sinc-shaped response of the V_{mean} vs magnetization (e.g. the solid curve in Figure 6B), that is, $V_{cut} = \pi/(2\gamma m_1)$ when assuming a laminar flow distribution within the imaging voxel.

For the labeling, V_{cut} is defined based on the magnetization difference (ΔM) after the control/label subtraction (Figure 6E,F). For non-FT labeling, the V_{cut} is chosen where ΔM first crossed $\Delta M = 1$, under the assumption of laminar flow (Figure 6F). This point is the first 0-crossing of the velocity response under the label condition (Figure 6B).[6] For FT-VSI, V_{cut} is also defined as the first crossing of $\Delta M = 1$,[30] but for the velocity response without an assumption of laminar flow (in a plug flow condition) (Figure 6E). This is also the 0-crossing or half-width-half-maximum point of FT-VSI's velocity response under the label condition (Figure 6C). These definitions are not the same, and other definitions are also possible and can be effective. We emphasize that in order for VSASL to quantitatively measure perfusion, V_{cut} for the labeling and the VCM should be matched, and defined in the same way. Looking forward, it will be useful to find an empirically accurate model for velocity distributions in the relevant vasculature so that a unified generic definition for V_{cut} can be used.

For the V_{cut}, a V_{mean} of 2 cm/s is recommended in both labeling and the VCM. This is a trade-off between the desired proximity of the labeling to the tissue and practical implementation considerations, such as minimizing EC sensitivity, diffusion attenuation artifacts, etc. (discussed below). Similarly, $V_{enc} = \pi/(\gamma m_1) = 4$ cm/s has been recommended for vascular crushing in PCASL,[1] which corresponds to the $V_{cut} = 2$ cm/s when using our definitions. No matter, which definition is used for labeling, once the RF pulses and the timings within the VS labeling module are determined, the V_{cut} is inversely proportional to the strength of the flow-sensitive gradients, and can be readily adjusted by scaling their amplitude.

9.2 | Direction of velocity-encoding gradients

The direction of the velocity-encoding gradients is recommended to be aligned with the major feeding vessels for applications in various organs. For the brain, superior–inferior (S-I) direction is therefore recommended

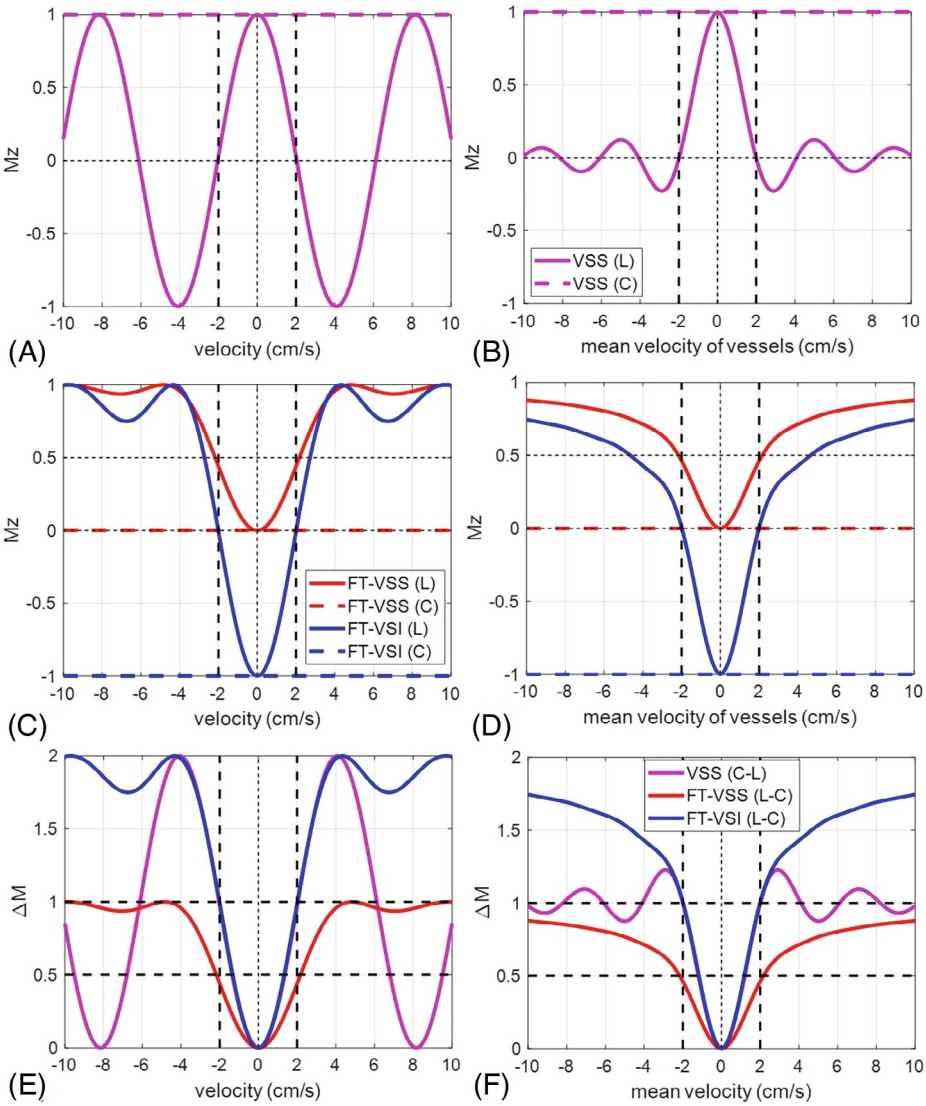

FIGURE 6 Simulated M_z-velocity responses of (A) velocity selective saturation (VSS) (magenta), (C) Fourier transform (FT)-VSS (red) and FT-velocity selective inversion (VSI) (blue), and (B, D) the corresponding results after the laminar flow integration (note that the x-axis is the mean velocity). The horizontal dashed lines are their magnetization responses under the control, respectively. Their arterial spin labeling (ASL) subtractions (ΔM) between label (L) and control (C) are displayed before (E) and after (F) laminar flow integration as well. V_{cut} is defined as the first crossing of $\Delta M = 1$, as indicated by the vertical black dotted lines at 2.0 cm/s (E,F). For VSS, the V_{cut} is chosen under the assumption of laminar flow (F). This point is the first 0-crossing of the velocity response under the label condition (B). For FT-VSI, V_{cut} can be defined without using laminar flow model (E). This is also the 0-crossing or half-width-half-maximum point of FT-VSI's velocity response under the label condition (C)

and has also been used most often in previous literature. V_{cut} below 4 cm/s for VSASL showed approximate isotropy with respect to the velocity-encoding directions.[6] However, some vessels in a plane perpendicular to the selected direction may not be efficiently labeled.

9.3 | Bolus duration (τ) and post-labeling delay

Although VS labeling is conceptually spatially nonselective, the VS pulse trains are still spatially constrained by the coverage of the RF transmitting coils and sensitivity to the B_1^+ field inhomogeneity, which determine the maximal bolus. Using multi-delay VSASL with a single sym-BIR-8 VSS labeling module, the maximal possible τ was estimated in a small group of young, healthy volunteers to be about 2.0 s in the brain when using a whole-body RF transmit coil for labeling.[21] This time could be longer in regions affected by vascular stenosis or shorter in patients with high flow. For cerebrovascular applications in adult populations at 3T, $\tau = 1.4$ s is recommended to optimize quantification accuracy and SNR efficiency.[21] PLD is typically set to 0, but could be increased to allow more time for the labeled bolus to move further down the vascular tree.

9.4 | Labeling efficiency (α)

Labeling efficiencies (α) of VS pulse are 0.5 for perfect VSS (because of saturation compared to inversion labeling) and 1.0 for perfect VSI, but are affected by multiple factors in real implementations. T_2 relaxation during the VS pulse train causes arterial signal decay, that is, $\exp(-eTE/T_{2,blood})$. The effective TE (eTE) is close to the full duration of VSS and half of the duration of FT-VSI.[15,30] This is because of the difference in time that the magnetization spends in the transverse

plane during these 2 pulse trains. For example, assuming $T_{2,blood}$ = 150 ms at 3T, T_2 attenuates efficiency by a factor of 0.87 for a 24 ms VSS pulse train (eTE = 21 ms), and 0.79 for a 64 ms FT-VSI pulse train (eTE = ~35 ms), respectively.[30]

Other major factors affecting α include the sensitivity to B_0 and B_1^+ inhomogeneities across the labeling volume. The sensitivity to B_0 inhomogeneities has been largely minimized by robust refocusing pulses and/or phase cycling (for VSI). Except for BIR-8-based VSS, the α of other VS labeling modules are affected by B_1^+ inhomogeneity because of the use of B_1-sensitive pulses for excitation pulses.[30] For example, given a B_1^+ scaling factor, for DRHS/T, the saturation degree for label can be calculated to be equal to $\cos^2(B_1^+ \times 90°)$ and therefore, subtracting label from control would result in $1\text{-}\cos^2(B_1^+ \times 90°) = \sin^2(B_1^+ \times 90°)$; for FT-VSI, the inversion degree for the control is $\cos(B_1^+ \times 180°)$ and subtracting control from label is $1\text{-}\cos(B_1^+ \times 180°) = 2 \times \sin^2(B_1^+ \times 90°)$. When normalized to respective saturation or inversion, the α of DRHS/T and FT-VSI have the same reduction factor of $\sin^2(B_1^+ \times 90°)$. Consequently, the inherent spatial variation of B_1^+ will result in a corresponding spatial variation of α. The mean overall reduction of α because of B_0 and B_1^+ inhomogeneities has been recently reported in a preliminary study using Bloch simulation and in vivo brain imaging[30]: ~6% for sym-BIR-8 VSS and ~29% for FT-VSI labeling using PCASL as the reference. Combining the T_2 attenuation and this reduction factor because of sensitivity to field inhomogeneities, α was estimated to be 0.41 and 0.56 for typical sym-BIR-8 VSS and FT-VSI (e.g., rect-VSI and sinc-VSI) pulse trains.[15,29,30]

Other factors may also contribute to labeling efficiency loss, such as temporal variations of velocities[15] and rapid flow of large vessels in the presence of local susceptibility gradients.[42] These effects are likely to apply for all VS labeling pulses and merit further investigation. VSMRA with 0 TI can help assess the labeling efficiency in large vessels.[28,42,43]

9.5 | Quantification of VSASL

With a PLD of 0, the blood flow (BF, in mL/100 g/min) can be quantified based on the kinetic model[44] as:

$$BF = \frac{6000 \cdot \lambda \cdot \Delta S \cdot e^{\frac{TI}{T_{1,blood}}} \cdot SI_B}{2 \cdot \alpha \cdot \tau \cdot SI_{PD}}, \quad (1)$$

where λ is the blood-tissue-partition coefficient (0.9 mL/g for the brain),[45] ΔS is the signal difference between the label and control images. Note that whether ΔS is subtracting label from control or subtracting control from label depends on both the control/label modules (VSS or FT-VSI) and the number of BS inversion pulses (even or odd) applied. As shown in Figure 3, τ is the bolus duration, or the time between labeling and VCM. TI is the time between labeling pulse and readout. $T_{1,blood}$ is the T_1 value of blood. Additional signal attenuation because of BS should also be included as a scaling factor in the equation above. A signal reduction of 5% for each BS pulse used is typical.[1] A separately acquired proton density (PD) image provides the signal intensity (SI) of tissue at equilibrium, SI_{PD}, for calibration. The VCM is recommended to be included in the PD image to cancel out the additional T_2 weighting. Otherwise, tissue T_2 decay during T_{VSS} needs to be accounted for as part of perfusion quantification. SI_B is the magnetization of the arterial blood right before labeling. When non-selective presaturation is used and we assume that all blood that will be labeled will have experienced this presaturation pulse (i.e., no fresh inflow), the magnetization of arterial blood will recover from saturation during T_{sat}:

$$SI_B = 1 - e^{\frac{-T_{sat}}{T_{1,blood}}}. \quad (2)$$

Slab-selective presaturation can be used in combination with sufficiently long T_{sat}, to allow fresh arterial blood with full magnetization to fill the vascular tree before applying the VS label or control module. In this case, $SI_B = 1$. Whether this holds true will depend on the specific VSASL parameter choices and expected CBF range and has not been fully studied, however.

9.6 | Recommended VSASL implementation

To summarize, the following elements are recommended for the implementation of a robust VSASL sequence at the time of writing (Figure 3), noting that this is still an evolving technique and future modifications and improvements are likely.

1. Readout: most readout schemes can work for VSASL acquisitions, however, 3D readouts have been found to be favorable over 2D readouts because of the uniformity of background suppression.
2. Labeling pulse: several VS labeling approaches will work and provide reasonable results. The sym-BIR-8 VSS pulse is more robust to imperfections in B_0 and B_1^+, and to ECs. FT-VSI pulses, however, yield greater labeling efficiency if B_0 and B_1^+ fields are reasonably homogeneous (e.g., in the head). τ has been shown to be

TABLE 1 Recommended parameters for VSASL at 3T for CBF quantification

V_{cut} (cutoff velocity, w.r.t. V_{mean})	2.0 cm/s
Velocity encoding direction	Superior-inferior (S-I)
τ (bolus duration)	1.4 s
PLD (post-labeling delay)	0.0 s
α (labeling efficiency)	
VSS	0.41
FT-VSI	0.56

optimal near 1.4 s at 3T. A V_{cut} of 2 cm/s with specified definition (Figure 6) is recommended, with the direction of the velocity encoding gradients aligned with the main arteries feeding the tissue of interest.

3 Vascular suppression: for both 2D and 3D readouts, a sym-BIR-8 VSS-based VCM is recommended immediately before the readout to remove contributions from the intravascular signal and to determine the trailing edge of the labeling (input) function. The V_{cut} and the direction of the VCM should match those of the labeling pulse.

4 Background suppression: a minimum of 2 inversion pulses after the labeling are recommended for effective background suppression with timings chosen to null the static tissue in the organ of interest (e.g., gray and white matter in the brain). In the case of VSI labeling, the inversion effect of the labeling pulse itself should be taken into account in calculating the timings for background suppression pulses.

5 Quantification: perfusion quantification can be achieved using the model specified by Equations (1) and (2), and the constants specified in Table 1. Note that an additional spin density image is required for quantification, the same as used in spatially selective ASL. A global saturation pulse is also recommended at the beginning of the TR to reset the magnetization for quantification accuracy.

9.7 | Other challenges of VSASL

Although robust velocity responses in the presence of B_0/B_1^+ field inhomogeneities are the primary focus when evaluating different VS pulse trains, their sensitivity to EC effects, diffusion attenuation, CSF contamination, and bulk motion also deserve attention.

VSASL is sensitive to ECs because of the non-identical gradient configurations between label and control modules. This can lead to artifactual signals in the perfusion weighted images because the magnetization of static spins will be differently affected during the 2 modules. EC errors can be evaluated using numerical simulations, as well as in phantoms for scanner-specific examinations.[15,18,19,29,30] Typically, EC artifacts mainly manifest along the direction of the velocity-encoding gradients used in the VS pulse trains and are more severe further from the isocenter. However, the severity of these EC-induced artifacts are also affected by B_0/B_1^+ field inhomogeneities,[29] which can make it difficult to recognize these artifacts in vivo. Sensitivity to ECs can be mitigated by optimizing the configurations of both the gradients[46] and the refocusing pulses,[6,15,18,19,29] in addition to having longer gaps between them.[19] Both sym-BIR-8 VSS and FT-VSI with composite refocusing pulses have been demonstrated to have improved resistance to EC effects in the brain.[15,19,30]

For a velocity-insensitive control with no gradients applied, unbalanced diffusion weighting may be another source of error in perfusion quantitation. Because of the high diffusivity, this error is higher in CSF than in gray matter and white matter. This effect should be corrected for, especially when multiple VS modules are used for labeling.[21] Note that the typical configurations of VS labeling (G_+, $180°_a$, G_-, G_+, $180°_a$, G_-) and velocity-compensated control (G_+, $180°_a$, G_+, G_+, $180°_a$, G_+) may only partially balance the diffusion weighting. It is possible to exactly match the b-values by applying an alternative labeling (G_+, $180°_a$, G_+, G_-, $180°_a$, G_-),[47] but this configuration was found to be more susceptible to EC effects and is not commonly used in VSASL.

Another important source of contamination originates from the pulsatile motion of CSF throughout the cardiac cycle. Because the velocity distribution of intracranial CSF exhibits large spatial and temporal variations, CSF spins decelerating from above to below V_{cut} will also be labeled and erroneously contribute to the perfusion signal. VS labeling is also sensitive to higher orders of motion not only in pulsatile CSF-flow, but also in non-pulsatile CSF flow and cysts or other fluid collections. CSF contamination becomes considerably more problematic as patients age, lose brain volume, and expand their subarachnoid spaces. Perfusion evaluated in brain parenchyma adjacent to these regions will be overestimated, for example in the mesial temporal lobes. Cystic lesions may also demonstrate elevated VSASL signal, which could erroneously be interpreted as hyperperfusion and lead to misdiagnosis. Clinical use of VSASL must pay special attention to these sources of error.

VS labeling is also sensitive to bulk motion, such as gross subject motion of head or the rest of body, myocardial motion, or respiration-induced movement of the liver and kidneys.[48] As tissue moving above the V_{cut} will be labeled erroneously, this motion effect cannot be corrected by co-registration and is likely to corrupt the perfusion

estimation. Although background suppression can reduce typical motion-induced subtraction artifacts seen in ASL, it cannot mitigate labeled tissue artifacts caused by motion, because any tag-control difference will remain at the readout.

9.8 | Clinical applications: general considerations

The main advantage of VSASL is its insensitivity to arterial transit delays. Consequently, VSASL measures blood flow with higher accuracy than spatial-based ASL in pathology that significantly prolongs ATT. This includes steno-occlusive diseases such as acute ischemic stroke, moyamoya, carotid stenosis, and renal artery stenosis. However, recent data suggests that VSASL may also be more accurate assessing perfusion within certain types of tumors, presumably because of heterogeneous ATTs. More generally, blood velocities in feeding arteries tend to decrease with age (e.g., within the cervical arteries),[49] also prolonging ATT.

A second advantage of VSASL over spatial-based ASL is that no spatial labeling region needs to be identified. This becomes especially important when measuring blood flow in organs that have complex arrangements of feeding arteries, such as in the placenta or heart, in which a spatial labeling plane may be difficult (if not impossible) to define. Spatial-based labeling also becomes challenging as patients age, because feeding arteries become more tortuous, particularly in patients with atherosclerosis. VSASL becomes a more practical ASL approach in these scenarios.

Finally, there are many situations, in which both VSASL and spatial-based ASL are useful by providing complementary information. In steno-occlusive disease, for example, VSASL can provide accurate perfusion, whereas spatial-based ASL can be used to identify regions of stenosis/occlusion and collateral flow (by means of macrovascular ASL signal, also called arterial transit artifact).

10 | NEURO APPLICATIONS

10.1 | Neuroradiology

The clinical use of VSASL in neuroimaging is best realized in cerebrovascular processes that cause prolonged ATT. This includes acute ischemic stroke (because of large vessel occlusion) and chronic steno-occlusive diseases such as moyamoya, carotid stenosis, and intracranial atherosclerosis. In these pathologies, long ATTs occur in the setting of narrowed or occluded proximal arteries, resulting in reduced (or absent) antegrade flow and delayed retrograde flow through circuitous collateral pathways. Even in normal aging, however, ATT can lengthen because of low cardiac output and decreased blood velocity in cervical carotid and vertebral arteries.[49]

The major clinical application of VSASL, therefore, far has been measuring CBF in moyamoya, a disease characterized by progressive, often idiopathic narrowing of arteries supplying the brain.[50] These stenoses limit blood flow to distal vascular territories and can result in ischemia and stroke. As a compensatory mechanism to maintain CBF, moyamoya patients develop extensive collateral networks that can have ATTs of several seconds. Two studies have used VSASL to evaluate CBF in pediatric and adult moyamoya, with comparison to PASL and PCASL, respectively.[51,52] Results were validated against digital subtraction angiography[52] and Xenon CT.[51] In both studies, VSASL accurately measured perfusion despite very long ATTs, whereas spatial-based ASL using standard PLDs were not able to assess microvascular perfusion because the label had not yet been delivered to the brain parenchyma (Figure 7).

A recent preliminary study compared VSASL to PASL in patients with suspected cortical ischemia without large vessel occlusion.[53] Despite using white-paper suggested parameters, perfusion deficits on PASL had a 25% to 35% false positive rate, with symptoms in these cases ultimately not considered to be ischemic in etiology (based on final clinical assessment and/or short-term repeat imaging). Moreover, 100% of the PASL false positives had normal perfusion on VSASL, suggesting that spatial-based ASL can lead to error even without flow-limiting stenosis. VSASL, on the other hand, demonstrated an exceptional <1% false positive rate for this cohort. More rigorous investigation as to whether VSASL can more accurately detect true ischemia is necessary and currently underway.

More recently, VSASL has been applied for imaging tumor perfusion in patients with gliomas (the most common primary malignant brain tumor in adults).[54] Gliomas typically demonstrate abnormal vascularity because of disorganized angiogenesis, potentially with regions of slow flow resulting in heterogeneous ATTs that could result in CBF underestimation with spatial-based ASL. In this study, VSASL-derived tumor blood flow better correlated with DSC perfusion imaging compared to PCASL and better distinguished low-grade and high-grade gliomas than PCASL. The study highlights the potential for VSASL to improve diagnostic performance of ASL in preparative grading of gliomas, presumably by minimizing transit delay sensitivity.

Certain pathologies will introduce complex blood flow patterns that deviate from the monotonically decelerating arterial blood flow on which VSASL theory is based. For

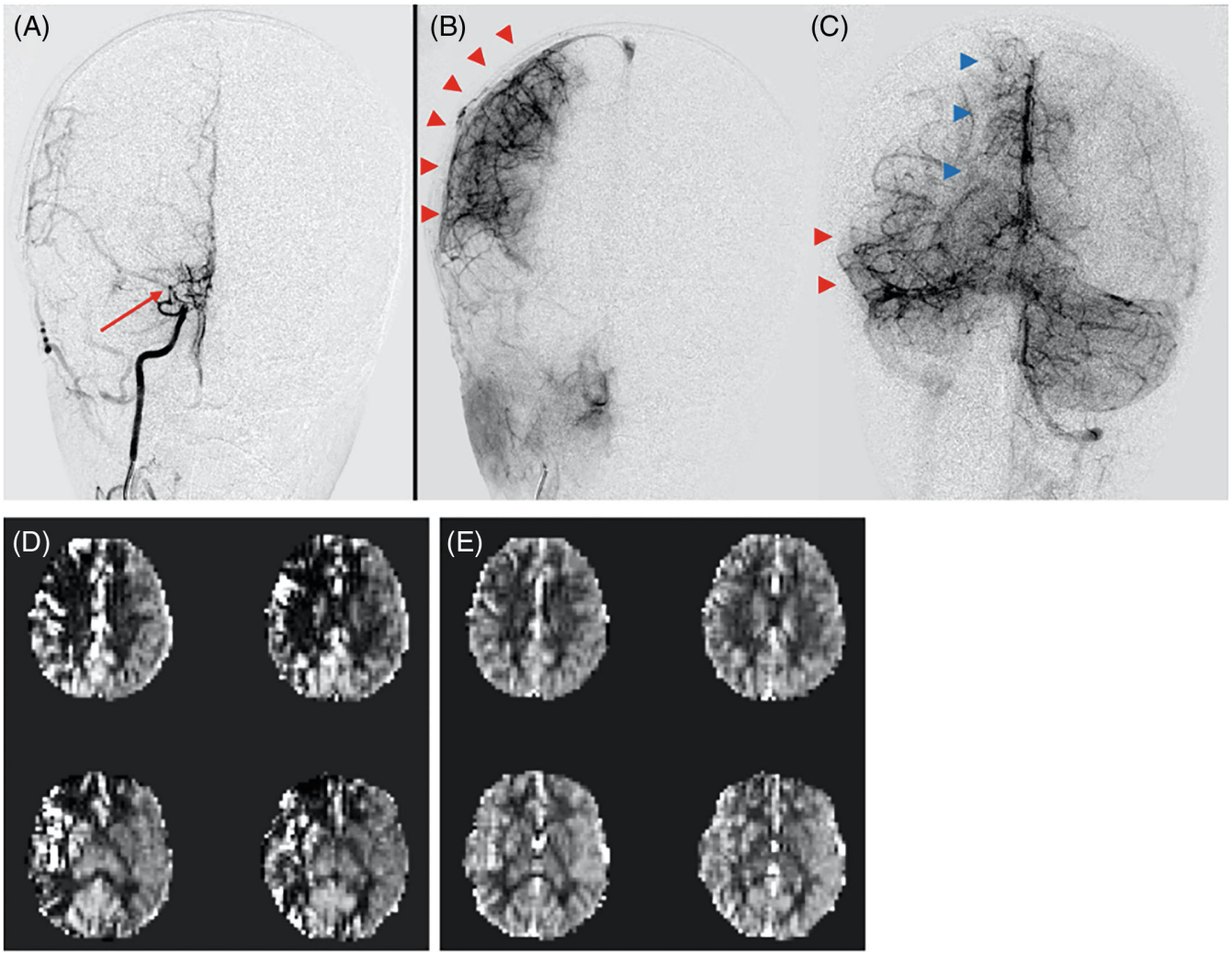

FIGURE 7 A 6-year-old with right-sided moyamoya status post successful revascularization (Matsushima A). (A) Cerebral angiogram during a right ICA injection demonstrates high-grade stenosis of the right ICA terminus, MCA origin, and ACA origin (red arrow), with nearly absent antegrade filling/ perfusion of the distal brain parenchyma. (B) Most of the right MCA territory (red arrowheads) is perfused through surgical collaterals via the ECA. (C) Remainder of the MCA (red arrowheads) and ACA (blue arrowheads) territories are perfused by native collaterals via the posterior circulation (left vertebral artery injection). (D) Traditional pulsed arterial spin labeling (PASL) fails to capture this perfusion because of prolonged arterial transit time (ATT)s through the collateral pathways; artifactual perfusion deficits and macrovascular signals are seen. (E) Velocity selective ASL (VSASL) accurately captures perfusion in these territories and is concordant with the angiogram

example, arterial stenosis seen in stroke, carotid stenosis, and moyamoya, can result in "jet" type physiology, with very slow and very fast flow within small spatial region. Similarly, disorganized, heterogeneous vasculature seen in tumors can result in turbulent and tortuous flow, also with interspersed high and low velocity regions. Our experience, therefore, far has suggested that VSASL remains accurate in these settings despite heterogeneous flow patterns, likely because of a sufficient blood volume decelerating from above to below V_{cut}. CBF underestimation and macrovascular artifacts, however, can theoretically arise; as our experience with VSASL in different pathologies deepens, we will become increasingly aware of situations that compromise accuracy.

VSASL fills a clear clinical need for accurate CBF measurements that are robust under a wide range of neuropathology. This is predominantly because of insensitivity to both ATT and orientation/tortuosity of feeding arteries, which are variable across patient populations and can dramatically bias spatial-based ASL. Despite improved quantitative accuracy, VSASL does not capture any information related to arterial transit, which can be useful in its own right. As mentioned above, a combined VSASL/PCASL approach[55] for steno-occlusive disease may be optimal to assess perfusion and stenosis/collaterals. Arteriovenous malformations or fistulae may also benefit from a combined approach for detecting arteriovenous shunting with high sensitivity.

10.2 | Cerebrovascular reactivity

Cerebrovascular reactivity (CVR) reflects the capacity of the brain to meet different physiological demands and can be applied to assess the risk of cerebrovascular diseases.[56] CVR can be obtained in a brain "stress test," in which CBF is measured before and after the administration of a vasodilator, such as acetazolamide.[57] Because 2 measurements of CBF are required to quantify CVR, ASL can be potentially a practical modality for CVR imaging.

For PCASL, the underestimation of baseline perfusion at brain regions with ATT longer than PLD (i.e., occipital lobe) could yield overestimated CVR. With a low sensitivity to transit time, VSASL may be a more suitable choice for CVR studies than standard ASL. A study that compared the CVR measurements using acetazolamide between VSASL and ^{15}O-water PET showed that VSASL was effective in measuring CVR in gray matter, but reported lower CVR than PET results.[58] VSASL was recently investigated in a CO_2-induced hypercapnia study and also observed lower CVR than phase-contrast MRI results.[59] It was found that, for VSASL, the underestimation of perfusion post-acetazolamide or during hypercapnia at brain regions where the trailing edge of the labeled bolus arrives before the application of VCM (i.e., frontal lobe) could yield underestimated CVR, similar to the issue of pulsed ASL.[60] This issue can be alleviated using a shorter PLD for VSASL,[59] to make it a clinically viable technique to screen patients with a higher risk of cerebrovascular diseases.

10.3 | Functional VSASL

ASL has long held great promise for functional MRI. Early work demonstrated that ASL offers important advantages over BOLD, but is hampered by low SNR and acquisition speed. These advantages include temporal stability (not subject to 1/f noise, which plagues BOLD functional MRI fMRI), and quantitation.[61–64]

Perfusion and blood volume fMRI have also been shown to be more specific to the parenchyma than BOLD, which can be more sensitive to superficial draining veins. This higher specificity permits layer specific fMRI,[65–68] although ASL is still not widely adopted for fMRI because of its low SNR and acquisition speed.

VSASL holds significant promise to overcome these issues. Repetition times can be reduced significantly in VSASL given the reduced TI required. By creating velocity and spatially selective labeling pulses, TRs as low as 400 ms have been achieved with high functional sensitivity.[69] This approach outperformed the speed of fast spatially selective ASL fMRI approaches.[70]

ATT in spatially selective ASL is significantly reduced during neuronal activation, which can obfuscate the quantified perfusion response.[71] In contrast, ATT is insignificant in VSASL, eliminating this confound.

Therefore, the SNR, speed, and reduced sensitivity to ATT of VSASL make it a promising candidate for perfusion-based fMRI experiments.[72] Indeed, recent work demonstrated improved sensitivity and specificity of VSASL over PCASL for a simple visuomotor paradigm.[36]

11 | BODY APPLICATIONS

The great promise of ASL for body applications is the subject of a companion paper. VSASL has been explored for a number of extracranial applications.

11.1 | Kidney

In the kidneys, there are 2 major advantages for using VSASL compared to PCASL and flow-sensitive alternating inversion recovery (FAIR) PASL. The first advantage is the reduced sensitivity to transit delays,[73] which is especially beneficial in patients with renal artery stenosis.[74] The optimal TI of 1200 ms for VSASL is slightly shorter than used in PCASL and FAIR.[73]

The second advantage is that no separate planning of the labeling plane is required. Respiratory motion can be challenging for the planning of the labeling region in FAIR and PCASL.[75] Initial experience[48,73] found that to minimize effects of respiratory motion on the labeling, the VS-gradient orientation should be in anterior–posterior or right–left direction and with a V_{cut} of 10.7 cm/s, higher than we recommend in the brain, although this V_{cut} may be too high for direct labeling of vasculature in the medulla. Image acquisition should be planned in coronal–oblique orientation parallel to the muscles anterior to the kidney to minimize through-slice motion.[48] Free-breathing acquisition is possible when image registration is used.[32]

At 3T, VSS-, mm-VSASL-, AccASL-, and FT-VSI-based ASL all showed similar perfusion weighted signal and tSNR to PCASL with good corticomedullary contrast in both cortex and medulla, but had significantly lower tSNR than FAIR. FT-VSI-ASL showed the most promising results,[32] and could benefit from acquisition at lower field strengths with smaller field inhomogeneities.

11.2 | Heart

Similar to kidney ASL, the 2 major advantages to VS labeling are: (1) reduced sensitivity to transit delay, which is a major consideration because many disease processes lead

to slow coronary flow and/or circuitous coronary collateral circulation; and (2) ease of scan planning.

Velocity selective human myocardial ASL has been demonstrated in 2 recent studies,[31,76] first with VSS pulses, and later with improved performance using FT-based pulse trains. One key design consideration was the velocity range of labeled blood versus background tissue. In a beating heart, even so-called "stable" cardiac phases involve a fair amount of normal tissue movement on the order of 1 to 2 cm/s. This is much larger than in other ASL target tissues (e.g., brain, kidney, and placenta). Coronary blood velocity is also extremely pulsatile with a peak velocity that varies substantially with disease (~20 cm/s in health, can be 100 cm/s in hypertension). Fortunately, the timing of peak coronary velocity and stable tissue velocity coincide at mid-diastole. This makes VS-labeling during mid-diastole a natural choice. Myocardial VSASL has shown promising results in healthy subjects, but has not yet been tested in large animal models of coronary artery disease, in patients, or in the context of stress testing.

11.3 | Placenta

The placenta is a vital organ for transferring oxygen and nutrients from the mother to the fetus via blood flow during pregnancy. Placental perfusion imaging using ASL, therefore, may provide early markers of placental dysfunction. There are 2 important characteristics in the placenta, which make VSASL a well-suited method for the organ. First, the placenta has highly tortuous arterial blood paths, multiple feeding arteries, and contributions from both maternal and fetal sides. Using conventional ASL, it may be difficult to find an optimal labeling region. In contrast, VSASL not only avoids such difficulties, but also achieves higher SNR because of labeling closer to the imaging region. Second, the placenta has exceptionally high blood volume (~50%) and small extravascular space, and therefore, the mean transit time of the labeled water is likely shorter. As a result, VSASL may provide more accurate perfusion measurements than conventional ASL because in this method, the arrival time of the labeled bolus is spatially uniform (0 in principle). Initial placental VSASL studies have demonstrated higher SNR than PCASL and reported significant perfusion differences between high- and low-risk pregnancies.[77,78] Further optimization of cut-off velocity, velocity encoding direction, VS labeling and image readout is warranted and currently under study.[79,80]

11.4 | Lung

The lung plays an important physiological role as the site of gas exchange between the blood and inspired air. Critical to this function is the match between the regional distributions of ventilation and perfusion, and ASL provides a non-invasive means of mapping the perfusion distribution.[81–83] In most tissues, there is a large extravascular fluid compartment that serves as a reservoir, into which labeled water can accumulate, effectively integrating the labeled bolus as it arrives and allowing for straightforward quantitation of perfusion from the ASL signal. In the lung, there is very little extravascular fluid to support this accumulation, and the use of spatially selective labeling with a long PLD to minimize intravascular artifacts will likely result in outflow of labeled blood into the venous circulation, compromising quantitative accuracy of the pulmonary perfusion measurement. In contrast, the velocity selective nature of VSASL is likely to make the delivery time to the capillary bed more uniform, allowing for more accurate timing of image acquisition to avoid outflow of the label. An initial effort in lung VSASL was reported earlier.[84]

12 | OTHER APPLICATIONS

Different VS pulse trains have also been used in various pulse sequences to characterize large vessels or quantify other hemodynamics parameters.

12.1 | Magnetic resonance angiography

VS pulse trains have been used for VSMRA as well. VSS pulse trains have been used for 3D black blood MRI[85–87] and subtraction-based bright blood MRA.[88–90] Recently, FT-VS pulse trains have been used before acquisition as a non-subtractive method for VSMRA. The angiographic signal is achieved by setting the flowing spins to be within the pass-band and static spins to be within either the inversion-band or saturation-band, therefore, it preserves flowing blood signal and avoids misregistration artifacts associated with subtractive approaches. This approach was first applied for abdominal[26] and peripheral[27] VSMRA at 1.5T with no or only a single refocusing pulse per velocity-encoding step. Later paired and phase-cycled refocusing pulses were incorporated into the FT-VS pulse trains for improved immunity to B_0/B_1 field inhomogeneities and were used for cerebral[28,33,34,91] and abdominal[92] VSMRA at 3T.

12.2 | Blood volume mapping

When interleaved VS label and control modules were applied right before acquisition without any labeling delay,

the vascular signal could be isolated by subtracting out the static tissue signal.[93] VSS pulse trains have been used for quantitative measurements of different compartments of cerebral blood volume (CBV),[93] for example, arterial CBV,[10,94] total CBV,[47] and venous CBV.[95] For total CBV measurement, the FT-VSS pulse train demonstrated better performance than both conventional VSS and BIR-8 pulse trains,[96] which might be related to its concurrent suppression of tissue background. Recently, the feasibility of FT-VS-based CBV and venous CBV estimation was demonstrated for 3D acquisition with large spatial coverage.[97] To label most microvessels, the cutoff velocity required for CBV quantification is considerably lower than typically used in CBF mapping (e.g., 0.35 vs 2.0 cm/s). Care should be taken to mitigate CSF contamination as well as unbalanced diffusion weighting.

12.3 | Venous oxygenation mapping

A powerful feature of VS labeling is the ability to specifically target signals from the venous blood compartment. This allows voxel-wise assessment of venous oxygen saturation based on measurement of T_2, and consequently the cerebral metabolic rate of oxygen. These approaches overcome limitations of the T_2 relaxation under spin tagging (TRUST) method, which permits only global or large-vessel measurements.[98,99]

The quantitative imaging of extraction of oxygen and tissue consumption (QUIXOTIC) method introduced by Bolar et al[100] uses 2 VSS modules to isolate accelerated venous blood in venules, from which venous oxygenation can be measured. Subsequent improvements result in dramatically shorter imaging times[101] and significantly increased SNR by nulling arterial signal without venous signal attenuation.[102] An important limitation of QUIXOTIC is potential contamination from CSF (as with other VSASL methods) and overestimation of venous oxygenation. The velocity selective excitation with arterial nulling (VSEAN) method developed by Guo and Wong[103] addresses this confound by using VS excitation to directly acquire signal from slow-moving venous spins, eliminating the need for individual control-label acquisition and subtraction. This results in improved SNR, scan efficiency, and quantitative accuracy (because there is reduced CSF contamination). Both QUIXOTIC and VSEAN have been applied in fMRI to measure the baseline and functional change of oxygenation in the brain regionally.[101,104] Recently, a new venous oxygenation mapping technique by using FT-VSI plus non-selective inversion to null the arterial blood signal while using FT-VSS to suppress the tissue signal was proposed with the advantage of higher venous signal.[105]

13 | SUMMARY

VSASL offers distinct advantages over traditional spatial-based ASL methods. First, VSASL is insensitive to arterial transit delays, permitting accurate blood flow measurement in settings of prolonged ATT, in which spatial-based ASL may fail. Second, VSASL permits perfusion measurement in regions where spatial labeling plane may be difficult to define. Despite these strengths, VSASL is limited by technical challenges that are gradually being overcome. We have reviewed here the current status of VSASL; made recommendations for the labeling, acquisition, modeling, quantification, and application; and highlighted progress and needs for further advancement. Wide dissemination of methods and evaluation in a range of clinical and research applications is still needed to further define the practical use and benefits of VSASL to the field of perfusion imaging.

DATA AVAILABILITY STATEMENT

During the Member Initiated Tutorial of VSASL (Velocity-Selective ASL: From Theory to Practice) at the Annual Meeting of ISMRM 2022 at London, England, United Kingdom, in addition to a series of comprehensive lectures, a hands-on session on Bloch equation simulation of VS labeling was also provided with the MATLAB code, which can be downloaded from: https://github.com/JosephGWoods/ISMRM2022_VSASL_Bloch_Simulations.

ORCID

Qin Qin https://orcid.org/0000-0002-6432-2944
Luis Hernandez-Garcia https://orcid.org/0000-0003-3002-0304
Dapeng Liu https://orcid.org/0000-0002-4432-3202
Krishna S. Nayak https://orcid.org/0000-0001-5735-3550
Sophie Schmid https://orcid.org/0000-0003-0750-7798
Matthias J. P. van Osch https://orcid.org/0000-0001-7034-8959
Joseph G. Woods https://orcid.org/0000-0002-0329-824X
Moss Y. Zhao https://orcid.org/0000-0002-0210-7739
Zungho Zun https://orcid.org/0000-0002-7297-3990
Jia Guo https://orcid.org/0000-0003-3371-5857

REFERENCES

1. Alsop DC, Detre JA, Golay X, et al. Recommended implementation of arterial spin-labeled perfusion MRI for clinical applications: a consensus of the ISMRM perfusion study group and the European consortium for ASL in dementia. *Magn Reson Med*. 2015;73:102-116.

2. Haller S, Zaharchuk G, Thomas DL, Lovblad KO, Barkhof F, Golay X. Arterial spin labeling perfusion of the brain: emerging clinical applications. *Radiology*. 2016;281:337-356.
3. Dai W, Garcia D, de Bazelaire C, Alsop DC. Continuous flow-driven inversion for arterial spin labeling using pulsed radio frequency and gradient fields. *Magn Reson Med*. 2008;60:1488-1497.
4. Alsop DC, Detre JA. Reduced transit-time sensitivity in non-invasive magnetic resonance imaging of human cerebral blood flow. *J Cereb Blood Flow Metab*. 1996;16:1236-1249.
5. Fan AP, Guo J, Khalighi MM, et al. Long-delay arterial spin labeling provides more accurate cerebral blood flow measurements in Moyamoya patients: a simultaneous positron emission tomography/MRI study. *Stroke*. 2017;48:2441-2449.
6. Wong EC, Cronin M, Wu WC, Inglis B, Frank LR, Liu TT. Velocity-selective arterial spin labeling. *Magn Reson Med*. 2006;55:1334-1341.
7. Wong EC, Buxton RB, Frank LR. Quantitative imaging of perfusion using a single subtraction (QUIPSS and QUIPSS II). *Magn Reson Med*. 1998;39:702-708.
8. Maki JH, Macfall JR, Johnson GA. The use of gradient flow compensation to separate diffusion and microcirculatory flow in Mri. *Magn Reson Med*. 1991;17:95-107.
9. Ye FQ, Mattay VS, Jezzard P, Frank JA, Weinberger DR, McLaughlin AC. Correction for vascular artifacts in cerebral blood flow values measured by using arterial spin tagging techniques. *Magn Reson Med*. 1997;37:226-235.
10. Petersen ET, Lim T, Golay X. Model-free arterial spin labeling quantification approach for perfusion MRI. *Magn Reson Med*. 2006;55:219-232.
11. Norris DG, Schwarzbauer C. Velocity selective radiofrequency pulse trains. *J Magn Reson*. 1999;137:231-236.
12. Wong EC, Liu TT, Sidaros K, Frank LR, Buxton RB. Velocity selective arterial spin labeling. Proceedings of the Annual Meeting of the ISMRM; 2002: 621; Honolulu, Hawai'i, USA.
13. Duhamel G, de Bazelaire C, Alsop DC. Evaluation of systematic quantification errors in velocity-selective arterial spin labeling of the brain. *Magn Reson Med*. 2003;50:145-153.
14. Reese TG, Heid O, Weisskoff RM, Wedeen VJ. Reduction of eddy-current-induced distortion in diffusion MRI using a twice-refocused spin echo. *Magn Reson Med*. 2003;49:177-182.
15. Qin Q, van Zijl PC. Velocity-selective-inversion prepared arterial spin labeling. *Magn Reson Med*. 2016;76:1136-1148.
16. Wong EC, Guo J. BIR-4 based B1 and B0 insensitive velocity selective pulse trains. Proceedings of the Annual Meeting of the ISMRM; 2010: 2853; Stockholm, Sweden.
17. Garwood M, Ke Y. Symmetric pulses to induce arbitrary flip angles with compensation for RF inhomogeneity and resonance offsets. *J Magn Reson*. 1991;94:511-525.
18. Meakin JA, Jezzard P. An optimized velocity selective arterial spin labeling module with reduced eddy current sensitivity for improved perfusion quantification. *Magn Reson Med*. 2013;69:832-838.
19. Guo J, Meakin JA, Jezzard P, Wong EC. An optimized design to reduce eddy current sensitivity in velocity-selective arterial spin labeling using symmetric BIR-8 pulses. *Magn Reson Med*. 2015;73:1085-1094.
20. Wong EC. New developments in arterial spin labeling pulse sequences. *NMR Biomed*. 2013;26:887-891.
21. Guo J, Wong EC. Increased SNR efficiency in velocity selective arterial spin labeling using multiple velocity selective saturation modules (mm-VSASL). *Magn Reson Med*. 2015;74:694-705.
22. Wong EC, Guo J. Velocity selective inversion pulse Trains for Velocity Selective Arterial Spin Labeling. Proceedings of the Annual Meeting of the ISMRM; 2009: 619; Honolulu, Hawai'i, USA.
23. Pauly J, Nishimura D, Macovski A. A k-space analysis of small-tip-angle excitation. *J Magn Reson*. 1989;81:43-56.
24. Pauly J, Nishimura D, Macovski A. A linear class of large-tip-angle selective excitation pulses. *J Magn Reson*. 1989;82:571-587.
25. de Rochefort L, Maitre X, Bittoun J, Durand E. Velocity-selective RF pulses in MRI. *Magn Reson Med*. 2006;55:171-176.
26. Shin T, Worters PW, Hu BS, Nishimura DG. Non-contrast-enhanced renal and abdominal MR angiography using velocity-selective inversion preparation. *Magn Reson Med*. 2013;69:1268-1275.
27. Shin T, Hu BS, Nishimura DG. Off-resonance-robust velocity-selective magnetization preparation for non-contrast-enhanced peripheral MR angiography. *Magn Reson Med*. 2013;70:1229-1240.
28. Qin Q, Shin T, Schär M, Guo H, Chen H, Qiao Y. Velocity-selective magnetization-prepared non-contrast-enhanced cerebral MR angiography at 3 tesla: improved immunity to B0/B1 inhomogeneity. *Magn Reson Med*. 2016;75:1232-1241.
29. Liu D, Xu F, Li W, van Zijl PC, Lin DD, Qin Q. Improved velocity-selective-inversion arterial spin labeling for cerebral blood flow mapping with 3D acquisition. *Magn Reson Med*. 2020;84:2512-2522.
30. Guo J, Das S, Hernandez-Garcia L. Comparison of velocity-selective arterial spin labeling schemes. *Magn Reson Med*. 2021;85:2027-2039.
31. Landes V, Javed A, Jao T, Qin Q, Nayak K. Improved velocity-selective labeling pulses for myocardial ASL. *Magn Reson Med*. 2020;84:1909-1918.
32. Franklin SL, Bones IK, Harteveld AA, et al. Multi-organ comparison of flow-based arterial spin labeling techniques: spatially non-selective labeling for cerebral and renal perfusion imaging. *Magn Reson Med*. 2021;85:2580-2594.
33. Shin T, Qin Q, Park JY, Crawford RS, Rajagopalan S. Identification and reduction of image artifacts in non-contrast-enhanced velocity-selective peripheral angiography at 3T. *Magn Reson Med*. 2016;76:466-477.
34. Shin T, Qin Q. Characterization and suppression of stripe artifact in velocity-selective magnetization-prepared unenhanced MR angiography. *Magn Reson Med*. 2018;80:1997-2005.
35. Liu D, Li W, Xu F, Zhu D, Shin T, Qin Q. Ensuring both velocity and spatial responses robust to B0/B1+ field inhomogeneities for velocity-selective arterial spin labeling through dynamic phase-cycling. *Magn Reson Med*. 2021;85:2723-2734.
36. Hernandez-Garcia L, Nielsen JF, Noll DC. Improved sensitivity and temporal resolution in perfusion MRI using velocity selective inversion ASL. *Magn Reson Med*. 2019;81:1004-1015.
37. Liu DP, Jiang DR, Tekes A, et al. Multi-parametric evaluation of cerebral hemodynamics in neonatal piglets using non-contrast-enhanced magnetic resonance imaging methods. *J Magn Reson Imaging*. 2021;54:1053-1065.

38. Priest AN, Taviani V, Graves MJ, Lomas DJ. Improved artery-vein separation with acceleration-dependent preparation for non-contrast-enhanced magnetic resonance angiography. *Magn Reson Med*. 2014;72:699-706.
39. Schmid S, Ghariq E, Teeuwisse WM, Webb A, van Osch MJ. Acceleration-selective arterial spin labeling. *Magn Reson Med*. 2014;71:191-199.
40. Schmid S, Petersen ET, Van Osch MJP. Insight into the labeling mechanism of acceleration selective arterial spin labeling. *Magn Reson Mater Phy*. 2017;30:165-174.
41. Schmid S, Heijtel DF, Mutsaerts HJ, et al. Comparison of velocity- and acceleration-selective arterial spin labeling with [15O]H2O positron emission tomography. *J Cereb Blood Flow Metab*. 2015;35:1296-1303.
42. Holmes JH, Jen ML, Eisenmenger LB, Schubert T, Turski PA, Johnson KM. Spatial dependency and the role of local susceptibility for velocity selective arterial spin labeling (VS-ASL) relative tagging efficiency using accelerated 3D radial sampling with a BIR-8 preparation. *Magn Reson Med*. 2021;86:293-307.
43. Xu F, Zhu D, Fan H, et al. Magnetic resonance angiography and perfusion mapping by arterial spin labeling using Fourier transform-based velocity-selective pulse trains: examination on a commercial perfusion phantom. *Magn Reson Med*. 2021;86:1360-1368.
44. Buxton RB, Frank LR, Wong EC, Siewert B, Warach S, Edelman RR. A general kinetic model for quantitative perfusion imaging with arterial spin labeling. *Magn Reson Med*. 1998;40:383-396.
45. Herscovitch P, Raichle ME. What is the correct value for the brain—blood partition coefficient for water? *J Cereb Blood Flow Metab*. 1985;5:65-69.
46. Woods JG, Wong EC, Shin DD, Bolar DS. A general framework for eddy current minimization in velocity selective arterial spin labeling. Proceedings of the Annual Meeting of the ISMRM; 2021:2720.
47. Liu D, Xu F, Lin DD, van Zijl PC, Qin Q. Quantitative measurement of cerebral blood volume using velocity-selective pulse trains. *Magn Reson Med*. 2017;77:92-101.
48. Bones IK, Franklin SL, Harteveld AA, et al. Influence of labeling parameters and respiratory motion on velocity-selective arterial spin labeling for renal perfusion imaging. *Magn Reson Med*. 2020;84:1919-1932.
49. Scheel P, Ruge C, Schoning M. Flow velocity and flow volume measurements in the extracranial carotid and vertebral arteries in healthy adults: reference data and the effects of age. *Ultrasound Med Biol*. 2000;26:1261-1266.
50. Scott RM, Smith ER. Moyamoya disease and moyamoya syndrome. *N Engl J Med*. 2009;360:1226-1237.
51. Qiu D, Straka M, Zun Z, Bammer R, Moseley ME, Zaharchuk G. CBF measurements using multidelay pseudocontinuous and velocity-selective arterial spin labeling in patients with long arterial transit delays: comparison with xenon CT CBF. *J Magn Reson Imaging*. 2012;36:110-119.
52. Bolar DS, Gagoski B, Orbach DB, et al. Comparison of CBF measured with combined velocity-selective arterial spin-labeling and pulsed arterial spin-labeling to blood flow patterns assessed by conventional angiography in pediatric Moyamoya. *Am J Neuroradiol*. 2019;40:1842-1849.
53. Bolar DS, Rosen BR, Schaefer PW. Comparison of velocity-selective and pulsed ASL perfusion MRI in patients with suspected cerebral cortical ischemia. Abstract with Oral Presentation of 56th Annual Meeting American Society of Neuroradiology; 2018; Vancouver, British Columbia, Canada.
54. Qu Y, Kong D, Wen H, et al. Perfusion measurement in brain gliomas using velocity-selective arterial spin labeling: comparison with pseudo-continuous arterial spin labeling and dynamic susceptibility contrast MRI. *Eur Radiol*. 2022;32:2976-2987.
55. Woods JG, Wong EC, Boyd EC, Bolar DS. VESPA ASL: VElocity and SPAtially selective arterial spin labeling. *Magn Reson Med*. 2022;87:2667-2684.
56. Markus H, Cullinane M. Severely impaired cerebrovascular reactivity predicts stroke and TIA risk in patients with carotid artery stenosis and occlusion. *Brain*. 2001;124:457-467.
57. Zhao MY, Vaclavu L, Petersen ET, et al. Quantification of cerebral perfusion and cerebrovascular reserve using turbo-QUASAR arterial spin labeling MRI. *Magn Reson Med*. 2020;83:731-748.
58. Zhao MY, Fan AP, Chen DYT, et al. Cerebrovascular reactivity measurements using simultaneous O15-water PET and ASL MRI: impacts of arterial transit time, labeling efficiency, and hematocrit. *NeuroImage*. 2021;233:117955.
59. Xu F, Xu C, Liu D, Xhu D, Lu H, Qin Q. Comparison of velocity selective ASL and PCASL with phase-contrast MRI for measuring CO_2-induced cerebrovascular reactivity. Proceedings of the Annual Meeting of the ISMRM; 2022: 4907; London, England, UK.
60. Tancredi FB, Gauthier CJ, Madjar C, et al. Comparison of pulsed and pseudocontinuous arterial spin-labeling for measuring CO_2-induced cerebrovascular reactivity. *J Magn Reson Imaging*. 2012;36:312-321.
61. Aguirre GK, Detre JA, Zarahn E, Alsop DC. Experimental design and the relative sensitivity of BOLD and perfusion fMRI. *NeuroImage*. 2002;15:488-500.
62. Wang J, Aguirre GK, Kimberg DY, Detre JA. Empirical analyses of null-hypothesis perfusion fMRI data at 1.5 and 4 T. *NeuroImage*. 2003;19:1449-1462.
63. Aguirre GK, Detre JA, Wang J. Perfusion fMRI for functional neuroimaging. *Int Rev Neurobiol*. 2005;66:213-236.
64. Borogovac A, Habeck C, Small SA, Asllani I. Mapping brain function using a 30-day interval between baseline and activation: a novel arterial spin labeling fMRI approach. *J Cerebr Blood F Met*. 2010;30:1721-1733.
65. Diekhoff S, Uludag K, Sparing R, et al. Functional localization in the human brain: gradient-Echo, spin-Echo, and arterial spin-labeling fMRI compared with neuronavigated TMS. *Hum Brain Mapp*. 2011;32:341-357.
66. Ivanov D, Gardumi A, Haast RAM, Pfeuffer J, Poser BA, Uludag K. Comparison of 3T and 7T ASL techniques for concurrent functional perfusion and BOLD studies. *NeuroImage*. 2017;156:363-376.
67. Huber L, Uludag K, Moller HE. Non-BOLD contrast for laminar fMRI in humans: CBF, CBV, and CMRO2. *NeuroImage*. 2019;197:742-760.
68. Chai Y, Li L, Huber L, Poser BA, Bandettini PA. Integrated VASO and perfusion contrast: a new tool for laminar functional MRI. *NeuroImage*. 2020;207:116358.
69. Bolar DS, Polimeni J, Ohringer N, Adalsteinsson E, Rosen BR. Turbo VSASL: slice-and velocity-selective ASL for high temporal resolution functional CBF mapping. Proceedings of the Annual Meeting of the ISMRM; 2018: 710; Paris, France.

70. Wong EC, Luh WM, Liu TT. Turbo ASL: arterial spin labeling with higher SNR and temporal resolution. *Magn Reson Med*. 2000;44:511-515.
71. Lee GR, Hernandez-Garcia L, Noll DC. Functional imaging with turbo-CASL: transit time and multislice imaging considerations. *Magn Reson Med*. 2007;57:661-669.
72. Wu WC, Wong EC. Feasibility of velocity selective arterial spin labeling in functional MRI. *J Cerebr Blood F Met*. 2007;27:831-838.
73. Bones IK, Franklin SL, Harteveld AA, et al. Exploring label dynamics of velocity-selective arterial spin labeling in the kidney. *Magn Reson Med*. 2021;86:131-142.
74. Safian RD, Textor SC. Renal-artery stenosis. *N Engl J Med*. 2001;344:431-442.
75. Nery F, Buchanan CE, Harteveld AA, et al. Consensus-based technical recommendations for clinical translation of renal ASL MRI. *MAGMA*. 2020;33:141-161.
76. Jao TR, Nayak KS. Demonstration of velocity selective myocardial arterial spin labeling perfusion imaging in humans. *Magn Reson Med*. 2018;80:272-278.
77. Zun ZH, Zaharchuk G, Andescavage NN, Donofrio MT, Limperopoulos C. Non-invasive placental perfusion imaging in pregnancies complicated by fetal heart disease using velocity-selective arterial spin labeled MRI. *Sci Rep UK*. 2017;7:16126.
78. Zun ZH, Limperopoulos C. Placental perfusion imaging using velocity-selective arterial spin labeling. *Magn Reson Med*. 2018;80:1036-1047.
79. Harteveld AA, Hutter J, Franklin SL, et al. Systematic evaluation of velocity-selective arterial spin labeling settings for placental perfusion measurement. *Magn Reson Med*. 2020;84:1828-1843.
80. Hutter J, Harteveld AA, Jackson LH, et al. Perfusion and apparent oxygenation in the human placenta (PERFOX). *Magn Reson Med*. 2020;83:549-560.
81. Mai VM, Berr SS. MR perfusion imaging of pulmonary parenchyma using pulsed arterial spin labeling techniques: FAIRER and FAIR. *J Magn Reson Imaging*. 1999;9:483-487.
82. Bolar DS, Levin DL, Hopkins SR, et al. Quantification of regional pulmonary blood flow using ASL-FAIRER. *Magn Reson Med*. 2006;55:1308-1317.
83. Henderson AC, Prisk GK, Levin DL, Hopkins SR, Buxton RB. Characterizing pulmonary blood flow distribution measured using arterial spin labeling. *NMR Biomed*. 2009;22:1025-1035.
84. Guo J, Wong EC. Pulmonary blood flow measurement using velocity-selective arterial spin labeling at 3.0T. Proceedings of the Annual Meeting of ISMRM; 2013: 6823; Salt Lake City, Utah, USA.
85. Sirol M, Itskovich VV, Mani V, et al. Lipid-rich atherosclerotic plaques detected by gadofluorine-enhanced in vivo magnetic resonance imaging. *Circulation*. 2004;109:2890-2896.
86. Koktzoglou I, Li D. Diffusion-prepared segmented steady-state free precession: application to 3D black-blood cardiovascular magnetic resonance of the thoracic aorta and carotid artery walls. *J Cardiovasc Magn Reson*. 2007;9:33-42.
87. Wang J, Yarnykh VL, Yuan C. Enhanced image quality in black-blood MRI using the improved motion-sensitized driven-equilibrium (iMSDE) sequence. *J Magn Reson Imaging*. 2010;31:1256-1263.
88. Fan Z, Sheehan J, Bi X, Liu X, Carr J, Li D. 3D noncontrast MR angiography of the distal lower extremities using flow-sensitive dephasing (FSD)-prepared balanced SSFP. *Magn Reson Med*. 2009;62:1523-1532.
89. Fan Z, Hodnett PA, Davarpanah AH, et al. Noncontrast magnetic resonance angiography of the hand: improved arterial conspicuity by multidirectional flow-sensitive dephasing magnetization preparation in 3D balanced steady-state free precession imaging. *Investig Radiol*. 2011;46:515-523.
90. Priest AN, Graves MJ, Lomas DJ. Non-contrast-enhanced vascular magnetic resonance imaging using flow-dependent preparation with subtraction. *Magn Reson Med*. 2012;67:628-637.
91. Li W, Xu F, Schar M, et al. Whole-brain arteriography and venography: using improved velocity-selective saturation pulse trains. *Magn Reson Med*. 2018;79:2014-2023.
92. Zhu D, Li W, Liu D, et al. Non-contrast-enhanced abdominal MRA at 3T using velocity-selective pulse trains. *Magn Reson Med*. 2020;84:1173-1183.
93. Hua J, Liu P, Kim T, et al. MRI techniques to measure arterial and venous cerebral blood volume. *NeuroImage*. 2019;187:17-31.
94. van Westen D, Petersen ET, Wirestam R, et al. Correlation between arterial blood volume obtained by arterial spin labelling and cerebral blood volume in intracranial tumours. *Magn Reson Mater Phy*. 2011;24:211-223.
95. Lee H, Wehrli FW. Venous cerebral blood volume mapping in the whole brain using venous-spin-labeled 3D turbo spin echo. *Magn Reson Med*. 2020;84:1991-2003.
96. Qin Q, Qu Y, Li W, et al. Cerebral blood volume mapping using Fourier-transform-based velocity-selective saturation pulse trains. *Magn Reson Med*. 2019;81:3544-3554.
97. Li W, Liu D, van Zijl PCM, Qin Q. Three-dimensional whole-brain mapping of cerebral blood volume and venous cerebral blood volume using Fourier transform-based velocity-selective pulse trains. *Magn Reson Med*. 2021;86:1420-1433.
98. Lu HZ, Ge YL. Quantitative evaluation of oxygenation in venous vessels using T2-relaxation-under-spin-tagging MRI. *Magn Reson Med*. 2008;60:357-363.
99. Krishnamurthy LC, Liu P, Ge Y, Lu H. Vessel-specific quantification of blood oxygenation with T2-relaxation-under-phase-contrast MRI. *Magn Reson Med*. 2014;71:978-989.
100. Bolar DS, Rosen BR, Sorensen AG, Adalsteinsson E. QUantitative imaging of eXtraction of oxygen and TIssue consumption (QUIXOTIC) using venular-targeted velocity-selective spin labeling. *Magn Reson Med*. 2011;66:1550-1562.
101. Stout JN, Adalsteinsson E, Rosen BR, Bolar DS. Functional oxygen extraction fraction (OEF) imaging with turbo gradient spin echo QUIXOTIC (turbo QUIXOTIC). *Magn Reson Med*. 2018;79:2713-2723.
102. Schmid S, Petersen ET, Hendrikse J, Webb A, van Osch MJP. Improved selection of the venous blood pool for OEF determination: IQ-OEF. Proceedings of the Annual Meeting of the ISMRM; 2012: 2008; Melbourne, Australia.
103. Guo J, Wong EC. Venous oxygenation mapping using velocity-selective excitation and arterial nulling. *Magn Reson Med*. 2012;68:1458-1471.

104. Liu EY, Guo J, Simon AB, Haist F, Dubowitz DJ, Buxton RB. The potential for gas-free measurements of absolute oxygen metabolism during both baseline and activation states in the human brain. *NeuroImage*. 2020;207: 116342.
105. Li W, Xu F, Zhu D, van Zijl PCM, Qin Q. T2-oximetry based cerebral venous oxygenation mapping using Fourier-transform based velocity-selective pulse trains. *Magn Reson Med*. 2022; 88:1292-1302.

How to cite this article: Qin Q, Alsop DC, Bolar DS, et al. Velocity-selective arterial spin labeling perfusion MRI: A review of the state of the art and recommendations for clinical implementation. *Magn Reson Med*. 2022;88:1528-1547. doi: 10.1002/mrm.29371